Multi-depth and refined detection method of karst features under thick Quaternary sediments of subway lines

Maoxin Su (sumaoxin2019@163.com)
Geotechnical and Structural Engineering Research Center, Shandong University https://orcid.org/0000-0002-4718-4295

Min Han
Geotechnical and Structural Engineering Research Center

Peng Wang
Geotechnical and Structural Engineering Research Center

Xiaoyin Ma
Geotechnical and Structural Engineering Research Center

Yimin Liu
School of GeoSciences, The University of Edinburgh

Research Article

Keywords: The thick Quaternary sediments, Karst, Integrated geophysical detection, 3D imaging, PCA, Data fusion,

Posted Date: March 24th, 2022

DOI: https://doi.org/10.21203/rs.3.rs-1354325/v1

Abstract

When the subway engineerings cross the karst area, the unfavorable geology may bring many potential safety hazards to the subway design, construction and operation. There is a wide range of karst distribution in southwest China. Extremely irregular karst area is distributed in the strata along the subway lines. The Quaternary sediments are thick, which greatly increases the difficulty of detection. A multi-depth refined detection method of karst features under thick Quaternary sediments is proposed in this paper. Firstly, the karst cavities and fractures in the shallow stratum of the study area are determined by ground-penetrating radar (GPR). Secondly, the mid-deep resistivity cross-sections are delineated using surface electrical resistivity tomography (ERT) and transient electromagnetic method (TEM). The principal component analysis (PCA) is used to fuse the resistivity data. The three-dimensional imaging is established to delineate the distribution of karst anomalies. As the information obtained by PCA is more comprehensive, the accuracy of geophysical interpretation is improved. The multi-depth refined detection of karst under thick Quaternary sediments on subway lines is realized through integrated analysis. This method has been applied in Changsha Metro Line 3 and achieved good practical results. It is of great application value for the karst tunnel treatment and the safe excavation.

1 Introduction

With the rapid development of China's economy, the gradual expansion of the urbanization process, the construction of urban rail transit has reached its peak. Water conservancy and hydropower, underground projects in karst areas become a new focus of development. When the subway tunnel passes through the karst area, it might bring many geological disasters, such as surrounding rock deformation, water and mud inrush, collapse. These engineering hazards bring great difficulties in construction (Li et al. 2016; Shi et al. 2017). Karst areas are widely distributed in China, especially in southwestern China. There are extremely irregular karst caves distributed along the subway lines in the strata. The Quaternary sediments are thick, loose, water-rich and present a low resistivity distribution. It has the adverse effects of shielding and isolating current. The complexity of geology conditions makes it more challenging to high-precision detection results of geophysical methods, bringing potential safety hazards to the stability and reliability of urban subway construction (Chen 2002). Therefore, the problem of improving karst detection accuracy under thick Quaternary sediments needs to be solved urgently.

This research takes the section between Lingguandu Station and Fubu River Station of Changsha Metro Line 3. According to the preliminary drilling results, the distribution of karst caves in this section is developed irregularly, and the development range is extensive. Owing to the cover of the loose Quaternary sediments such as alluvial fan, diluvial fan and colluvial soil, making it difficult to determine the karst distribution. As the traditional drilling method has a high cost, long construction period and can only carry out single point exploration, it is challenging to locate the distribution of karst areas in thick Quaternary sediments by geological drilling alone. It is necessary to employ advanced and high-precision geophysical exploration methods. Geophysical exploration results contain more geological information with high exploration efficiency, which can verify and complement the traditional drilling methods (Li et

al. 2015; Kaufmann and Romanov 2016; Su et al. 2021c). Therefore, to accurately detect the spatial distribution and geological structure of karst caves under the condition of the Quaternary sediments, geological data should be combined, and geophysical exploration methods should be adopted.

At present, there are many geophysical methods used in karst exploration, such as surface electrical resistivity tomography (ERT), transient electromagnetic method (TEM), cross-hole ERT, ground-penetrating radar (GPR) (Baggett et al. 2020). Each approach has its strengths and limitations. A single detection method provides part of the characteristic information of karst and is challenging to achieve refined detection of karst. Multiple geophysical methods are combined to detect karst features to reduce the uncertainty of interpretation by a single detection method. Integrated geophysical detection results can effectively complement the detection depth, accuracy and anomaly reflection of different methods. Using this method can make full use of their advantages respectively, and make up for the shortcomings of each method in the detection. This combination improves the accuracy and reliability of the detection results. Different geophysical methods were used to interpret geological anomalies comprehensively. Afshar et al. (2015) conducted detection for the distribution range of underground cavity and groundwater using a combination of ground-penetrating radar and ERT method. Zhang et al. (2019) applied cross-hole ERT and cross-hole seismic tomography to detect underground karst in the urban subway and improve exploration accuracy. Su et al. (2021c) used GPR, TEM and three-dimensional (3D) laser scanning technology to provide a quantitative and integrated exploration of shallow karst distribution.

Considering the complexity of geological, geophysical characteristics, and site limitations in this bid section, GPR, surface ERT and TEM were adopted in the research. A method for multi-depth and refined detection of karst features under thick Quaternary sediments is proposed. Firstly, the principle, the advantages and disadvantages of the three methods and principal component analysis (PCA) were introduced. Then, the numerical simulation was carried out. The inversion results were fused based on PCA and generated the corresponding 3D detection results. In practice, GPR is used to locate cavities and fissures in shallow strata, and then surface ERT and TEM are used to detect the deeper part along the same survey line. The obtained resistivity data are fused by PCA. Finally, the 3D imaging of GPR and resistivity are drawn, respectively. The fused data combines the advantages of the two methods to reflect more comprehensive geological information. The multi-depth refined detection of karst features under thick Quaternary sediments is realized through integrated interpretation. Through the engineering example verification, this method was successfully applied to the treatment project in the Changsha Metro Line 3. It successfully overcomes the limitations of the single geophysical method and more accurately delineates the distribution range of the karst caves. It is beneficial to the prevention and control of karst disasters. This case study effectively provides critical guidance for the karst caves treatment scheme and the safety of subway tunnel excavation. This method has good application value.

2 Background On The Study Area

The study area is located between Lingguandu Station and Fubu River Station of Changsha Metro Line 3 (Fig. 1). This bid section starts at Fubu River Station. After leaving Fubu River Station, the subway line crosses Xiangjiang River and Juzizhou and finally goes about 100 m east along Laodong West Road to Lingguandu Station.

It is revealed by drilling that the upper stratum of this section is filled with plain fill, silty sand, gravel and silty clay. The bedrock is mainly dolomitic limestone, sandstone and conglomerate. The deepest buried depth of the karst cave is 45 m from the surface. There are six karst caves, and their height is bigger than 6 m, and the highest cave is 22.46 m. Most of the karst caves are filled. The filling materials are mainly sandy, pebbles and cohesive soil, and some are empty. The karst caves are densely developed in this section bid. The stratum crossed by the subway line is mainly moderately weathered sandstone, strongly weathered sandstone, moderately weathered conglomerate, strongly weathered conglomerate and moderately weathered limestone. The grade of surrounding rock is mainly V – VI.

The groundwater in the study area includes Quaternary unconsolidated strata pore water, layered bedrock fissure water and Carbonate rock fissure water. Based on the development characteristics of karst caves revealed by drilling and the analysis of water inflow from the borehole during the drilling process, this area has developed karst caves in the right line CK15 + 799.5 – CK16 + 112.52, and the karst range is relatively large. The fillings are mainly sand, gravel and pebble layers with strong water permeability, and there is no filling partly. It can be seen that the karst cave fillings have good water permeability and are rich in water. These karst caves have a hydraulic connection with the Xiangjiang River, and a wide range of water inrush water influx. The bedrock rocks are relatively complete, and the water abundance and permeability of the rock stratum are poor. Because the confined water of the karst cave and the upper phreatic water have a close hydraulic connection with the water of the Xiangjiang River, the tunnel construction is easy to cause groundwater gushing along the karst cave developed area.

Figure 1 Location of the study area

3 Methodology

Much research on karst geological exploration using geophysical methods has been carried out, and valuable results and conclusions have been obtained. Various geophysical methods have played a critical role in the forecast and early warning of karst disasters from different fields, such as electrical, magnetic and well logging (Chatelier et al. 2011). Given different engineering and geological conditions, the selection, combination and survey lines layout of exploration methods are designed.

3.1 Method selection

The upper stratum of this section is filled with soil, silty sand, pebble and silty clay. The bedrock is mainly dolomitic limestone, sandstone and conglomerate. The karst caves are mainly developed at the cracks of the bedrock surface, and on a large scale, covered by thick Quaternary sediments. It is difficult to accurately detect karst distribution in the thick coverage area. The reason is, firstly, the thick Quaternary

sediments have a strong absorption and attenuation effect on the reflection wave, which is not conducive to receiving the effective reflected signal in the stratum; secondly, in the process of Quaternary sedimentation, the sedimentary conditions are complex. There are many geological phenomena such as interlayer and interbedding, and it is easy to interfere with each other in the detection process of different stratum interfaces. GPR is a high-precision method in shallow subsurface detection fields. The geological structure changes are reflected as the opposite and weakening of reflected wave in-phase axis in GPR signal receiving (Cassidy et al. 2011; Liu et al. 2020). When air-filled cavities appear in the stratum, the dielectric constant is small, electromagnetic waves decay fast, and high resistivity will appear. When there is a water-filled cavity, its dielectric constant is generally large, the propagation speed of electromagnetic waves in water is fast, and the relative resistivity is low. It is difficult to determine the deep karst distribution and geological structure under thick overburden by GPR alone. Therefore, in the detection of thick Quaternary sediments area, it is not only required to use high-resolution GPR, but also need to adopt a step by step detection strategy corresponding to the depth to find out the distribution of karst area from shallow to deep.

When the filling in the cavity has good water permeability, there is an obvious difference between the resistivity of the filled cavity and the surrounding rocks. The electrical resistivity is low, especially when the cavity is filled with water (Yao et al. 2012). The resistivity is generally 20–100 Ω·m. Bedrock with good compactness typically has high resistivity value, mostly above 2000 Ω·m. So, the resistivity methods, such as surface ERT and TEM, based on electrical differences has been adopted to detect karst distribution. These methods are sensitive to low resistivity anomalies. Surface ERT has a noticeable detection resolution on mid-deep strata, but it is hard to identify the location of deep karst caves accurately (Gan et al. 2020). TEM has the ability to penetrate thick Quaternary sediments with low resistivity, and has a good detection result on deep strata (Huang et al. 2010). Surface ERT and TEM can obtain the distribution information and characteristics of formation resistivity on subway lines.

According to the analysis of known karst cave characteristics and geological data in the study area, the deepest buried depth of karst cave roof is 45 m. The karst caves are widely distributed. Therefore, the multi-depth and refined detection method for karst geology under thick Quaternary sediments used three methods: GPR, surface ERT and TEM. The three methods are combined and comprehensive interpretation to obtain richer stratum information and anomalous body response characteristics. The relationship and implementation process of each method are shown in Fig. 2.

Figure 2 Schematic of the technology roadmap multi-depth and refined detection method of karst features under thick Quaternary sediments of subway lines

3.2 Method and principle

The principles, application conditions, survey lines layout, detection depth and resolution of surface ERT, TEM and GPR are different. The principles and field implementation of these three methods are introduced. The principles and field implementation of the three methods are described below.

3.2.1 GPR method

GPR is an efficient shallow subsurface geophysical exploration technology, which adopts the difference of electrical parameters of underground media to infer media structure and physical properties by transmitting high-frequency electromagnetic pulse waves with a frequency of 106–109 Hz. With the continuous development of microelectronics and signal processing technology, GPR is widely used in many fields, such as geological engineering survey, building structure survey, highway engineering quality detection, underground pipeline detection, etc. (Demirci et al. 2012; Alani et al. 2013).

The basic principle of GPR is shown in Fig. 3. The transmitting antenna directionally sends the high-frequency short-pulse electromagnetic wave into the ground. When the electromagnetic wave encounters the stratum or target with electrical differences in the propagation process, it will be reflected and transmitted. The receiving antenna receives the reflected wave signal and digitizes it, which is then recorded by a computer as a reflected waveform (Wang 1993). The collected data are processed by direct wave removal, band-pass filtering and background removal. The spatial position, structure and distribution of underground targets can be realized according to the kinematic and dynamic characteristics such as propagation time, amplitude, waveform and frequency of a reflected wave. GPR delineates the underground targets based on the analysis of reflection waveform characteristics. As a result, its detection resolution mainly depends on the electrical difference between the underground target and the surrounding medium, the attenuation degree of electromagnetic wave, the buried depth of the targets, and the strength of external interference.

Figure 3 Schematic diagram of GPR method

3.2.2 Surface ERT method

Surface ERT is a resistivity exploration technology proposed in the 1980s (Dong and Wang 2003). Based on the difference of electrical parameters between the surrounding rock and water-bearing geological structure, surface ERT infers geological conditions and resistivity distribution in the detection area according to the distribution law of conduction current field in surrounding rock under the action of an applied electric field. Surface ERT has the advantages of sufficient data, low expense, little field interference, high work efficiency and convenient interpretation corresponding to the resistivity cross-sections. It is mainly used to detect the water content of the geological body, bedrock buried depth, concealed structure, fault, fracture zone, etc., and has achieved apparent geological effect and remarkable socioeconomic performance (Chen et al. 2017). However, it is difficult to carry out quantitative interpretation, which is greatly affected by topographic relief, and it is not convenient to employ in the exposed bedrock area.

The implementation of surface ERT is to arrange a certain number of electrodes in the detection area. The apparatus automatically supply direct current (A and B electrodes) according to a certain sequence, and measure the potential difference between the two electrodes (M and N electrodes), to calculate the apparent resistivity profiles (Dong and Wang 2003). Through the inversion of the apparent resistivity

profile, the resistivity distribution of surrounding rock is obtained. The basic principle of surface ERT is shown in Fig. 4. In the field observation, all electrodes are arranged at one time. The intelligent electrode converter and measuring instrument are used to realize the full-automatic data acquisition. The collected data are processed by computer, generating the resistivity section.

Figure 4 Schematic diagram of the surface ERT method, electrode arrangement and data processing flowchart

3.2.3 TEM method

TEM method is a time-domain electromagnetic method that employs the ungrounded loop to emit a pulsed magnetic field in front of the working face. When the current in the transmitter loop is suddenly switched off, the medium will induce the secondary magnetic field to maintain the primary field generated when the current is connected. The magnitude and attenuation characteristics of the secondary magnetic field are related to the electrical distribution of the surrounding medium. The variation characteristics of the secondary field with time are observed intermittently in the primary field. After processing, the electrical properties, scale, and occurrence of the underground medium can be understood to delineate the targets, as shown in Fig. 5 (Xue et al. 2007). TEM is employed to directly observe the secondary magnetic field, which greatly reduces the detection difficulty of the abnormal body, and its detection effect and ability have been greatly improved. It has the advantages of small effect, high vertical and horizontal resolution, sensitive response to low resistivity targets and fast arrangement. It is widely used in various engineering geophysical exploration. It is an ideal detection method to realize the detection of rich-water areas and engineering hydrogeology (Lin et al. 2016).

Figure 5 Schematic diagram of the TEM method

3.2.4 PCA data fusion

Data fusion combines data information from different sources (spatially or temporally redundant or complementary) to obtain a consistent interpretation or description of the detected target. In geosciences, many researchers favour PCA due to its advantages in extracting the main components of overlapping information. The PCA method was pioneered in 1901 and is widely used in image enhancement, image fusion, signal compression, and noise removal (Bajorski 2011; Hansen et al. 2014; Chen et al. 2020). Subsequently, PCA was applied to geophysical data fusion. Yin et al. (2008) used a nonlinear kernel function for the dimension reduction optimization of seismic data, achieving good data extraction performance. Lu (2018) denoised the airborne electromagnetic data through PCA, which enhanced the resolution of airborne electromagnetic exploration of deep underground anomalies. Therefore, the usage of PCA is based on the idea of dimension reduction. The purpose of resistivity data fusion is to combine the advantages of different methods in exploring different depths of the formation. On this basis, unified imaging results containing comprehensive information can be obtained through PCA fusion processing, thereby improving the utilization of geophysical data.

Based on the PCA transformation with an orthogonal linear relationship of information content, the data are projected into a new coordinate system using the linear projection method. The new component vector is distributed according to the information content, and the first principal component contains the most extensive information. The basic idea is to synthesize *p* observation variables into *p* new variables. For the *p*-dimensional sample observation data *x*, the PCA transformation process mainly includes standardization processing, calculating the sample correlation coefficient matrix, calculating the eigenvalues and eigenvectors of the correlation coefficient matrix by Jacobian method, and selecting important components. The corresponding eigenvector is the new coordinate base. In an actual analysis, not all *p* principal components are selected; instead, the first *k* principal components are selected according to the cumulative contribution rate (*CCR*) of each principal component. This contribution rate is defined by the eigenvalues λ in Eq. 1:

$$CCR = \frac{\lambda_i}{\sum_{i=1}^{p} \lambda_i} \quad (1)$$

A large contribution rate indicates that the corresponding principal component contains critical information regarding the original variable. Generally, the *CCR* of more than 85% is the threshold for selecting the principal component to ensure that the comprehensive variable includes the most information about the original variable. Finally, the *p*-dimensional vector is mapped to the selected *k*-dimensional coordinate space.

3.3 Numerical simulation analysis

In order to verify the response of GPR, surface ERT and TEM to stratigraphic boundary and anomalies, the corresponding geoelectric models were established for numerical simulation according to the drilling information. The area of the survey line (0–560 m) corresponds to the surface ERT model. The area enclosed by red the dashed box (265–294 m) in the survey line was used as the forward model of the GPR and TEM (Fig. 5). The parameters of the stratigraphic type, boundary depth, relative dielectric constant , and resistivity of each layer are shown in Table 1 according to the different layers from top to bottom.

Table 1 Numerical simulation model parameters

Stratigraphic type	Boundary depth (m)	Relative dielectric constant (ε_r)	Resistivity ρ (Ω·m)
Miscellaneous fill	3	14	150
Silty clay	6	9	70
Gravelly sand	10	4	500
Fine round gravel	16	5	700
Fully weathered conglomerate	34	10	1000
Intensely weathered conglomerate	40	8	2000
Cave	46	30	50
Moderately weathered conglomerate	65	7	5000

Table 1 Numerical simulation model parameters

Figure 6 Model of numerical simulation

In the GPR forward model, the excitation source was the Ricker wavelet with a dominant frequency of 100 MHz, and the sampling time window was 1100 ns. The interface depth can be calculated using the wave velocity and two-way travel time data of the reflected wave in the medium (Schultz 1982; Liu et al. 2018). The corresponding exploration depth is about 15 m. The grid spacing used was $\Delta x = 0.05$ m and $\Delta y = 0.05$ m. The transceiver antenna spacing was 0.5 m. The common offset was 0.5 m, and 56 records were generated. The waveform results after the direct wave removal, band-pass filtering, background removal and other processing is shown in Fig. 7. The figure shows that the shallow stratum (0–15 m) interfaces were well-reflected and high detection resolution. The deep stratum (15–65 m) reflected wave was weakened, and poor identification ability. Due to the little difference in the relative dielectric constant in the three stratums of 16–40 m, increasing depth, and the attenuation of electromagnetic waves, the deep stratum and karst cave's resolution is inaccurate. Therefore, GPR can detect cavities and fractures in near-surface anomalies.

As shown in Fig. 6, surface ERT forward modelling was conducted. The Wenner-Schlumberger array was used for the forward calculation. The total number of electrodes was 141, the unit electrode spacing was 4 m, and the horizontal survey line length was 560 m. The apparent resistivity data obtained by forward modelling were inverted. The inversion profile of the surface ERT was obtained through conventional

processing (see Fig. 8). The figure exhibits that surface ERT has four interfaces at a depth of 10, 16, 35, 47 meters. As the first three layers resistivity is relatively smaller than that of other stratums, the inversion result of these three stratums shows low resistivity and no interface response. However, it can be seen that the distribution of formation resistivity changed from low-high-low-high. The position of the formation interface could be roughly identified, as it was affected by gradual changes in the resistivity contour.

TEM method adopts a central loop. The equivalent radius of the transmitter loop was 30 m, the receiving loop was 1 m, and the number of coil turns was 10. The simulation result is shown in Fig. 9. The TEM response to the low resistivity anomalies is obvious in the figure. There is an apparent low-resistivity anomaly at 41–46m, and the change of resistivity is consistent with the model parameters. Due to the delay effect of transient electromagnetic, the shallow resolution is low, and it isn't easy to distinguish the specific horizon within a certain depth range (0–20m). Due to the delay effect of TEM, the near-surface resolution is low, and it is difficult to distinguish the specific layers within 0–20m.

Figure 7 Numerical simulation of eight stratums using GPR

Figure 8 Numerical simulation of eight stratums using surface ERT

Figure 9 Numerical simulation of eight stratums using TEM

According to the detection results, PCA is performed on the inversion resistivity data of the overlapped part of the survey line, and the fusion result is shown in Fig. 10. Compared with the TEM inversion result, the near-surface resolution of the fused image is improved, and the detection resolution of the deep karst cave is retained. Two low resistivity areas shown in the depths of 4–8 m and 41–46 m.

Figure 10 Cross-section after TEM and surface ERT inversion resistivity data fusion

4. Case Study Application

4.1 Field implementation

Applying the schematic of the technology roadmap (Fig. 2), the following mainly described the combination between different geophysical exploration methods and the layout scheme of survey lines. Among these three methods, the electrodes arrangement of surface ERT is flexible, which can obtain rich geological information and realize the automation of data acquisition. TEM adopted a point by point measurement, which has a large detection depth and simplified measurement work. The anomalies have a strong response in the low-resistivity surrounding rock area. GPR adopted the data acquisition of continuous measurement, which had high detection efficiency and high precision. It can realize a rapid measurement in a wide range of survey lines.

Surface ERT has a high lateral resolution. It has an apparent response to the low resistivity anomaly in the mid-deep stratum and can accurately reflect the position of the anomaly. TEM is sensitive to low

resistivity anomalies and can locate deep stratum. Combining the two methods is based on detection depth and accuracy requirements. Due to the turn-off time of TEM, there is a certain blind area in the shallow stratum. As a supplementary detection of TEM blind area, surface ERT is a direct current resistivity method to determine invisible anomalies or interfaces in underground mid-deep stratum (< 20m). Therefore, surface ERT and TEM were carried out along the same survey line in the study area. The resistivity data of the two methods are fused by PCA and performed by 3D imaging. The fused data obtained a more comprehensive information of anomalies and realized a multi-depth detection. Combining the two different methods related to depth resolution can complement and verify each other, which is conducive to improving the accuracy of individual preliminary exploration results. Then, GPR and 3D imaging are carried out in the same survey line to detect karst cavities and fractures in thick Quaternary sediments. Finally, the three methods are conducted to realize an integrated interpretation, which is verified by borehole information. Due to site restrictions, surface ERT cannot detect the middle of the survey area, which is the same starting point as the TEM and GPR survey lines. The layout of the field survey lines is shown in Fig. 11.

Figure 11 Layout of the survey line

4.2 GPR 3D imaging

Firstly, GPR is used to ascertain the geological conditions of thick Quaternary sediments, cavities and cracks in the shallow stratum. GPR prospecting used the SIR-4000 control unit with a 100 MHz transmitting antenna. The spacing of survey lines is 3.3 m. According to the difference in propagation velocity of the electromagnetic wave in propagation velocity in different media, the observation time window was selected to 500 ns, and the corresponding exploration depth is about 15 m. Other parameters are shown in Table 2. The 3D pseudo-colour waveform imaging was built up after trace editing, filtering and denoising, shown in Fig. 12. The karst fracture zone and cavity can be further identified and delineated in the 3D imaging. The reflected wave in the range of the black dotted box has strong reflection and large amplitude, so it is inferred that there may be geological anomalies in this range. In order to judge whether the anomalies are cavities or karst, 2D slice imaging is carried out on the 3D results (see Fig. 13). In Fig. 13, there is no apparent hyperbolic response and cavity, but muddy water scouring cracks cause chaotic reflections. The broken rock mass caused the discontinuity of the in-phase axis.

Table 2
Parameter preferences of GPR in detection

Transmitted power	Central frequency of transmitting antenna	Measuring mode	Average velocity of electromagnetic wave	Stacking times of signal
50 KHz	100 MHz	Time	0.06 m/ns	16

Table 2 Parameter of GPR in detection

Figure 12 3D pseudo-colour waveform results of GPR

Figure 13 2D GPR slice for detailed interpretation of geological structures at GL-4

4.3 3D imaging interpretation after resistivity data fusion

4.3.1. Surface ERT detection results

Based on the GPR 3D imaging, direct current resistivity exploration is adopted to detect karst under thick Quaternary sediments, providing necessary guidance for later grouting treatment. Surface ERT deployed a Wenner-Schlumberger array with a voltage of 24 V, and the electrode spacing was 2 m. The number of electrodes was 42, and each survey line length was 82m. The spacing of survey lines is 3.3 m. During the detection, the parameters of the four lines were the same. Other parameters are shown in Table 3. The resistivity results obtained after inversion are shown in Fig. 14. The figure shows that the shallow stratum (0–10 m) has high detection accuracy. Still, the edge at both ends of the survey line has a low resolution, and there is an inverted trapezoidal peripheral detection blind zone of surface ERT. It can be seen from EL-2 and EL-3 that the thickness of Quaternary sediments first increases and then decreases from northwest to southeast. There are thick Quaternary sediments in the middle of the survey line (32–60 m), the coverage depth is nearly 30 m, the Quaternary sediments at both ends of the survey line (0–32 m, 60–82 m) was thin, and the thickness was only 10 m. The thickness of Quaternary sediments varies greatly.

Table 3
Parameter preferences of surface ERT in detection

Device type	Voltage	Electrode spacing	Total number of electrodes	Line spacing	Number of layers
WDA-1	24V	2 m	168	3.3 m	13

Table 3 Parameter of surface ERT in detection

Figure 14 Surface ERT inversion section

4.3.2 TEM detection results

TEM adopted t a central loop. The side length of the transmitting loop is 2 m, and the receiving loop area is 31.4 m^2. Each survey line adopted the point measurement. The parameters of the four survey lines are the same during the detection process. The other parameters are shown in Table 4. The resistivity results obtained after 2D inversion of the TEM data are shown in Fig. 15. It can be seen from the figure that there were two low resistivity anomalies of survey line TL-2, one was 0–4 m in the survey line with a depth of 12–32 m, and the other was within the range of 22–29 m in the survey line with a depth of 12–30 m. There was a low resistivity anomaly at a depth of 30m of survey line TL-3. The overburden thickness was close to 40 m at the 25–29 m of survey line TL-4. The coverage range gradually increased along the survey line direction. The detection results of TEM were consistent with the results of surface ERT. It was inferred that a water-inrush channel was developed by the connection of karst fracture in the northeast-

southwest direction. In addition, the bedrock interface was mainly below 35 m, and the rock interface fluctuated greatly. Compared with the detection results of surface ERT, it can be found that the TEM method has high resolution in the deep stratum (10–65 m), and the detection resolution in the shallow stratum (0–10 m) is lower than surface ERT. Therefore, it is necessary to integrate TEM and surface ERT detection results.

Table 4 Parameter preferences of TEM in detection

Device type	Transmitter				Turn-off time	Receiver	Point spacing
Central loop	Size 2m×2m	Number of turns 64	Current 1A	Frequency 25Hz	50 μs	Receiving loop	1m

Table 4 Parameter of TEM in detection

Figure 15 TEM inversion results

4.3.3 Resistivity fusion 3D imaging

To make full use of the advantages of surface ERT and TEM and overcome their defects in detection depth, the overlapping part of survey line 0–29 m and depth 0–10 m were used for resistivity fusion through PCA. In order to make the detection results more intuitive, 3D imaging was established on the fused resistivity data, and the results are shown in Fig. 16. The figure shows that the thickness of Quaternary sediments varies greatly. The thickest part was up to 45 m, thin in the middle and thick on both sides. The rock interface fluctuated greatly. The main intact bedrock existed below 35 m, and the rock interface above 35 m is irregular. The rock was relatively broken, most of the rock was clay and strongly weathered rock. The stratigraphic distribution was complex. As the karst area was developed at the boundary of soil layers, it is inferred that it was mainly distributed at a depth of 30–45 m. In order to verify the accuracy of detection results, drilling was further carried out. The drilling location is shown in the Fig. 17. Samples were taken from ZK01, ZK02 and ZK03 boreholes respectively, and the borehole histogram was shown in Fig. 18. From the drilling core samples results, the overburden in the shallow part (0–7 m) was miscellaneous fill and silty clay. The water content was rich, showing low resistivity in the 3D resistivity imaging. The middle and deep part (7–30 m) was fine round gravel and conglomerate, and the resistivity was high. There was a through karst cave at the depth of 30–40 m. The karst cave of borehole ZK01 was distributed at a depth about 40 m, and the karst cave at ZK02 and ZK03 was about 30 m. This was consistent with the imaging results after data fusion. As the study area had a hydraulical connection with the Xiangjiang River and the overburden was rich in water, the middle and shallow (0–30 m) clay layer or rock fracture area would show a low resistivity distribution.

Figure 16 Resistivity fusion 3D imaging

Figure 17 Drilling position map of the study area

Figure 18 Drilling histograms of the engineering site: each drilling corresponds to the specific position in Fig. 17

4.4 integrated interpretation

For the same survey line in the study area, GPR, surface ERT, and TEM are carried out respectively. The cavities, fractures, and karst in the shallow stratum were outlined in the horizontal and vertical directions to provide a basis for subsequent governance. In the karst development area under thick Quaternary sediments, the geological conditions, spatial position and shape of the anomalies are complex. If 2D imaging was used alone, it is difficult to comprehensively and intuitively ascertain the spatial position and shape of the anomalies. Therefore, 3D imaging of the detection data is convenient for interpreting geophysical exploration results. Due to the existence of karst in underground fractures, fault zones and water-rich channels, the resistivity of natural rocks was reduced, made it apparently different from the resistivity of the surrounding strata. The difference of resistivity was used to identify the underground karst area. The resistivity data of surface ERT and TEM are fused for 3D visualization and imaging. Secondly, by adopting GPR to detect the cavities and cracks in the shallow stratum, the geological distribution of the karst area with thick Quaternary sediments was realized to achieve the multi-depth refined detection.

5. Discussion

The karst environment is one of the most challenging engineering and environmental issues in China. Geophysical exploration methods can provide useful information on the distribution of underground media in karst areas. For instance, water inflow estimation, groundwater exploration and risk assessment (Chalikakis et al. 2011; Ozel and Darici 2020; Su et al. 2021a). However, a karst area remains a challenging environment for geophysical exploration methods. The selection of the best-suited geophysical exploration method is not always straightforward due to the variable and unpredictable target characteristics, and each method has limitations. In karst detection under thick Quaternary sediments, the effective signal of seismic reflections is strongly absorbed, and the reflected signal is weak (Chalikakis 2006). GPR results supply a high-resolution near-surface imaging and thus provides relevant geological information such as stratifications and fractures. However, the investigation depth of the GPR remains about to 20 m (Carriere et al. 2013). The depth of GPR is greatly affected by different strata, especially in high-conductivity media such as clay, which reduces the penetration depth of GPR (Benson 1995). The effectiveness of surface ERT is limited by decreasing resolution with depth and no valid data near the ends of the survey line. Increasing the survey line length will increase depth of investigation but it may not be possible at urban sites where the space is limited (Kiflu et al. 2016). The electrodes may hard to not insert into the asphalt or concrete ground. TEM cannot detect shallow strata (Plotnikov 2014). Therefore, it is necessary to use comprehensive geophysical methods to detect

unfavourable geological targets (De Giorgi and Leucci 2014; Cueto et al. 2018). The integrated geophysical method is to process the observed different detection data and image them individually. The results are then compared and analyzed to determine the structural distribution and physical properties of underground rock strata from different properties. This analysis reduces the multiplicity of single geophysical results to a certain extent (Nie et al. 2020). However, this analysis lacks the internal relationship and correlation between different methods and makes insufficient use of rich geological information. At the same time, the result of individual imaging is easy to confuse anomalies analysis and geological interpretation, especially when survey lines are dense. The imaging and interpretation of geophysical results are more arduous. 3D imaging has great advantages when the survey lines are complex. The electrical properties of karst anomalies are different. Direct current electrical exploration is suitable for large-scale karst geological exploration. Surface ERT has the advantages of high lateral resolution, rich information and high detection efficiency (Samyn et al. 2014). The resistivity of karst is a low resistivity value compared to the surrounding rocks. The surface ERT and TEM detection results are presented in the resistivity profile. Surface ERT can make up for the shallow stratum detection blind area of TEM. TEM can make up for the disadvantages of surface ERT which is limited by the layout of survey lines and affected by topography (Su et al. 2021b). Therefore, the inversion resistivity data of the two methods can be fused. After fusion, the two methods achieve complementary advantages.

From the numerical simulation of surface ERT (Fig. 8), it can be seen that there is a boundary effect, and the resistivity becomes higher at the boundary of the profile. The resolution is poor (Akingboye and Ogunyele 2019). Due to the influence of the gradual change characteristics of resistivity contour, the formation interface only can be roughly distinguished. The thick Quaternary sediments have a shielding effect on direct current, resulting in the unclear response of deep low-resistivity anomalies. TEM can penetrate the high resistivity targets in the thick Quaternary sediments, so it has a good resolution on deep low resistivity anomalies (Li et al. 2017). After fusing, the resolution of shallow and deep stratum is improved (Fig. 10). In field test, due to site constraints, the survey line is not arranged in the middle of the survey line. The resistivity profile of surface ERT is inverted trapezoid (Loke and Barker 1995). There are detection blind areas at both ends of the survey line, reducing the detection accuracy. Moreover, the detection resolution of surface ERT for deep strata is poor. However, the delineation of resistivity anomalies is more refined through data fusion. Compared with the TEM detection results (Fig. 15), the shallow resolution is improved, which is consistent with the numerical simulation results.

The cavities and fissures in the thick Quaternary sediments provide a water channel connection for groundwater, so GPR is used for supplementary detection (Dorn et al. 2012; Liu et al. 2021). The water content greatly affects the dielectric constant of surrounding rock. The relative permittivity of karst areas, cavity and fissure are quite different from intact rock. 100MHz antenna is commonly used in the detection process, with a limited detection range. This is suitable for near-surface detection (Beres et al. 2001). The numerical simulation results show the shallow stratum boundary response is dinstinct (Fig. 7).

GPR, surface ERT and TEM are chosen to be comprehensively analyzed in this study. In the subsequent field application, it is necessary to select the optimal combination of geophysical exploration methods according to the engineering geological, geophysical characteristics and field conditions. The combination of the drilling verification and geological survey could effectively determine the development state and influence of karst anomalies that may cause geological disasters. There are many interference factors in practical engineering detection. To improve the fusion efficiency, it is necessary to preprocess the detection data to reduce the interference and improve the signal-to-noise ratio (Kim et al. 2007).

In this study, PCA was used to fuse the inversion results of different methods and 3D imaging, mainly considering the advantages of utilizing complementary information and simplifying redundant information. However, PCA is only applicable to linear dimensionality reduction, and the cumulative contribution rate of the first several principal components should reach a high level. With the development of the fusion theory, many fusion algorithms are proposed, such as wavelet analysis, kernel principal component analysis, HIS transforming (Cheng and Xiao 2006; Zhou et al. 2019). These methods have some applicability in geophysical exploration methods.

6. Conclusions

Aiming at detecting the karst features under thick Quaternary sediments on subway lines, a multi-depth refined comprehensive exploration method was proposed in this paper. Through numerical simulation and case study, the feasibility of this method is proved. This method mainly combines the advantages of surface ERT, TEM within different depths and PCA in data fusion. Considering the potential advantages of surface ERT and TEM in karst detection, the combination of surface ERT and TEM realizes supplementary verification. TEM data can supplement the blind area of inverted trapezoid detection of surface ERT. GPR was used to supplement and further detect karst caves, soil caves and cracks in shallow strata. The combination of the three geophysical methods can realize the multi-depth refined exploration of karst with thick Quaternary sediments. This method can realize a more intuitively and comprehensively understanding of the distribution of karst and cavities on the subway line. The successful application of this method in Lingguandu Station and Fubu River Station section of Changsha Metro Line 3 verifies the effectiveness of this method. It provides practical guidance for subway construction detection under the condition of thick Quaternary sediments.

Declarations

Acknowledgements: Much of the work presented in this paper was supported by the Shandong Provincial Natural Science Foundation (Grant number ZR2014EEM028, Grant number 2019GSF111028), National Natural Science Foundations of China (Grant number 41877239). The authors would like to express appreciation to the reviewers for their valuable comments and suggestions that helped improve the quality of our paper.

Author contribution:

All authors contributed to the study conception and design. Data collection and analysis were performed by MXS, MH, PW, XYM and YML. The first draft of the manuscript was written by MH and all authors commented on previous versions of the manuscript. All authors read and approved the final manuscript.

Funding: This research was supported by the Shandong Provincial Natural Science Foundation (Grant number ZR2014EEM028, Grant number 2019GSF111028), National Natural Science Foundations of China (Grant number 41877239).

Competing Interests:

The authors declare that they have no known competing financial interests or personal relationships that could have appeared to influence the work reported in this paper.

Author contribution:

All authors contributed to the study conception and design. Data collection and analysis were performed by MXS, MH, PW, XYM and YML. The first draft of the manuscript was written by MH and all authors commented on previous versions of the manuscript. All authors read and approved the final manuscript.

References

1. Afshar A, Abedi M, Norouzi GH, Riahi MA (2015) Geophysical investigation of underground water content zones using electrical resistivity tomography and ground penetrating radar: A case study in Hesarak-Karaj, Iran. Eng Geol 196:183–193. https://doi.org/10.1016/j.enggeo.2015.07.022
2. Akingboye AS, Ogunyele AC (2019) Insight into seismic refraction and electrical resistivity tomography techniques in subsurface investigations. Rud-Geol-Naft Zb 34:93–111. https://doi.org/10.17794/rgn.2019.1.9
3. Alani AM, Aboutalebi M, Kilic G (2013) Applications of ground penetrating radar (GPR) in bridge deck monitoring and assessment. J Appl Geophys 97:45–54. https://doi.org/10.1016/j.jappgeo.2013.04.009
4. Baggett J, Abbasi A, Monsalve J, Bishop R, Ripepi N, Hole J (2020) Ground-penetrating radar for karst detection in underground stone mines. Min Metall Explor 37:153–165. https://doi.org/10.1007/s42461-019-00144-1
5. Bajorski P (2011) Statistical inference in PCA for hyperspectral images. IEEE J-STSP 5:438–445. https://doi.org/10.1109/jstsp.2011.2105244
6. Benson AK (1995) Applications of ground-penetrating radar in assessing some geological hazards - examples of groundwater contamination, faults, cavities. J Appl Geophys 33:177–193. https://doi.org/10.1016/0926-9851(94)00029-n
7. Beres M, Luetscher M, Olivier R (2001) Integration of ground-penetrating radar and microgravimetric methods to map shallow caves. J Appl Geophys 46:249–262. https://doi.org/10.1016/s0926-9851(01)00042-8

8. Carriere SD, Chalikakis K, Senechal G, Danquigny C, Emblanch C (2013) Combining electrical resistivity tomography and ground penetrating radar to study geological structuring of karst unsaturated zone. J Appl Geophys 94:31–41. https://doi.org/10.1016/j.jappgeo.2013.03.014
9. Cassidy NJ, Eddies R, Dods S (2011) Void detection beneath reinforced concrete sections: The practical application of ground-penetrating radar and ultrasonic techniques. J Appl Geophys 74:263–276. https://doi.org/10.1016/j.jappgeo.2011.06.003
10. Chalikakis K (2006) Application de methodes geophysiques pour la reconnaissance et la
11. protection de ressources en eau dans les milieux karstiques. Dissertation, Universite Pierre-et-Marie-Curie, Paris-VI
12. Chalikakis K, Plagnes V, Guerin R, Valois R, Bosch FP (2011) Contribution of geophysical methods to karst-system exploration: An overview. Hydrogeol J 19:1169–1180. https://doi.org/10.1007/s10040-011-0746-x
13. Chatelier M, Ruelleu S, Bour O, Porel G, Delay F (2011) Combined fluid temperature and flow logging for the characterization of hydraulic structure in a fractured karst aquifer. J Hydrol 400:377–386. https://doi.org/10.1016/j.jhydrol.2011.01.051
14. Chen C, He X, Guo B, Zhao X, Chu Y (2020) A pixel-level fusion method for multi-source optical remote sensing image combining the principal component analysis and curvelet transform. Earth Sci Inform 13:1005–1013. https://doi.org/10.1007/s12145-020-00472-7
15. Chen M (2002) Cause analysis and quasi-quantitativ prediction on the collapse of karst overburden.Chin J Rock Mech Eng285–289
16. Chen S, Yu S, Liu H, Qi J, Liu D (2017) Application and research of high density resistivity method in hydrogeological prospectinga case study on Jiangping town map. Progress in Geophysiscs 32:849–855
17. Cheng Y, Xiao B (2006) Evaluation of data fusion algorithms. Comput Meas Control 14:937–941
18. Cueto M, Olona J, Fernandez-Viejo G, Pando L, Lopez-Fernandez C (2018) Karst-induced sinkhole detection using an integrated geophysical survey: A case study along the Riyadh Metro Line 3 (Saudi Arabia). Near Surf Geophys 16:270–281. https://doi.org/10.3997/1873-0604.2018003
19. Demirci S, Yigit E, Eskidemir IH, Ozdemir C (2012) Ground penetrating radar imaging of water leaks from buried pipes based on back-projection method. Ndt & E Int 47:35–42. https://doi.org/10.1016/j.ndteint.2011.12.008
20. De Giorgi L, Leucci G (2014) Detection of hazardous cavities below a road using combined geophysical methods. Surv Geophys 35:1003–1021. https://doi.org/10.1007/s10712-013-9277-4
21. Dong H, Wang C (2003) Development and application of 2D resistivity imaging surveys.Earth Sci Front171–176
22. Dorn C, Linde N, Doetsch J, Le Borgne T, Bour O (2012) Fracture imaging within a granitic rock aquifer using multiple-offset single-hole and cross-hole GPR reflection data. J Appl Geophys 78:123–132. https://doi.org/10.1016/j.jappgeo.2011.01.010

23. Gan J, Zhang Y, Xiao L (2020) An application of the high-density electrical resistivity method for detecting slide zones in deep-seated landslides in limestone areas. J Appl Geophys 177. https://doi.org/10.1016/j.jappgeo.2020.104013
24. Hansen TJ, Abrahamsen TJ, Hansen LK (2014) Denoising by semi-supervised kernel PCA preimaging. Pattern Recogn Lett 49:114–120. https://doi.org/10.1016/j.patrec.2014.06.015
25. Huang J, Deng J, Liu Q, Xie S, Chen H (2010) Application research of transient electromagnetic method in the underwater-karst detection. 4th International Conference on Environmental and Engineering Geophysics, Chengdu Univ Technol, Chengdu, China
26. Kaufmann G, Romanov D (2016) Structure and evolution of collapse sinkholes: Combined interpretation from physico-chemical modelling and geophysical field work. J Hydrol 540:688–698. https://doi.org/10.1016/j.jhydrol.2016.06.050
27. Kiflu H, Kruse S, Loke MH, Wilkinson PB, Harro D (2016) Improving resistivity survey resolution at sites with limited spatial extent using buried electrode arrays. J Appl Geophys 135:338–355. https://doi.org/10.1016/j.jappgeo.2016.10.011
28. Kim JH, Cho SJ, Yi MJ (2007) Removal of ringing noise in GPR data by signal processing. Geosci J 11:75–81. https://doi.org/10.1007/bf02910382
29. Li L, Xue J, Zhao X, Cao Q (2017) The exploration of mined-out areas by integrated geophysical method. Geophys Geochemical Explor 41:377–380
30. Li L, Tu W, Shi S, Chen J, Zhang Y (2016) Mechanism of water inrush in tunnel construction in karst area. Geomat Nat Haz Risk 7:35–46. https://doi.org/10.1080/19475705.2016.1181342
31. Li S, Zhou Z, Ye Z, Li L, Zhang Q, Xu Z (2015) Comprehensive geophysical prediction and treatment measures of karst caves in deep buried tunnel. J Appl Geophys 116:247–257. https://doi.org/10.1016/j.jappgeo.2015.03.019
32. Lin F, Chen S, Ma G (2016) Transient electromagnetic detection method in water-sealed underground storage caverns. Undergr Space 1:44–61. https://doi.org/10.1016/j.undsp.2016.07.001
33. Liu H, Shi Z, Li J, Liu C, Meng X, Du Y, Chen J (2021) Detection of road cavities in urban cities by 3d ground-penetrating radar. Geophysics 86:WA25–WA33. https://doi.org/10.1190/geo2020-0384.1
34. Liu M, Liu Z, Zhou D, Lan R, Wu H (2020) Recognition method of typical anomalies during karst tunnel construction using GPR attributes and gaussian processes. Arab J Geosci 13. https://doi.org/10.1007/s12517-020-05782-0
35. Liu T, Klotzsche A, Pondkule M, Vereecken H, Su Y, Van Der Kruk J (2018) Radius estimation of subsurface cylindrical objects from ground-penetrating-radar data using full-waveform inversion. Geophysics 83:H43–H54. https://doi.org/10.1190/geo2017-0815.1
36. Loke MH, Barker RD (1995) Least-squares deconvolution of apparent resistivity pseudosections. Geophysics 60:1682–1690. https://doi.org/10.1190/1.1443900
37. Lu Y (2018) Study on noise removal for airborne electromagnetic data based on principal component analysis and minimum noise fraction. Dissertation, Jilin University

38. Nie L, Zhang Y, Su M, Geng Y, Liu Z, Fan K, Yan B, Shen J (2020) Comprehensive ahead prospecting of tunnels in severely weathered rock mass environments with high water inrush risk: A case study in Shaanxi province. Adv Civ Eng 2020. https://doi.org/10.1155/2020/8867382
39. Ozel S, Darici N (2020) Environmental hazard analysis of a gypsum karst depression area with geophysical methods: A case study in Sivas (Turkey). Environ Earth Sci 79. https://doi.org/10.1007/s12665-020-8861-4
40. Plotnikov AE (2014) Evaluation of limitations of the transient electromagnetic method in shallow-depth studies: Numerical experiment. Russ Geol Geophys 55:907–914. https://doi.org/10.1016/j.rgg.2014.06.009
41. Samyn K, Mathieu F, Bitri A, Nachbaur A, Closset L (2014) Integrated geophysical approach in assessing karst presence and sinkhole susceptibility along flood-protection dykes of the Loire river, Orleans, France. Eng Geol 183:170–184. https://doi.org/10.1016/j.enggeo.2014.10.013
42. Schultz PS (1982) A method for direct estimation of interval velocities. Geophysics 47:1657–1671. https://doi.org/10.1190/1.1441315
43. Shi S, Bu L, Li S, Xiong Z, Xie X, Li L, Zhou Z, Xu Z, Ma D (2017) Application of comprehensive prediction method of water inrush hazards induced by unfavourable geological body in high risk karst tunnel: A case study. Geomat Nat Haz Risk 8:1407–1423. https://doi.org/10.1080/19475705.2017.1337656
44. Su M, Li C, Xue Y, Wang P, Cheng K, Liu Y (2021a) Engineering application of fuzzy evaluation based on comprehensive weight in the selection of geophysical prospecting methods. Earth Sci Inform. https://doi.org/10.1007/s12145-021-00701-7
45. Su M, Liu Y, Xue Y, Nie L, Wang P, Li C, Ma X (2021b) Integrated geophysical detection of water inrush from foundation pit near the river: A case study of Nanjing subway station. Environ Earth Sci 80. https://doi.org/10.1007/s12665-021-10015-y
46. Su M, Zhao Y, Xue Y, Wang P, Xia T, Zhang K, Li C (2021c) Progressive fine integrated geophysical method for karst detection during subway construction. Pure Appl Geophys 178:91–106. https://doi.org/10.1007/s00024-020-02636-4
47. Wang H (1993) An introduction to ground penetrating radar-preface and postscript to the current special issue.Earth Science249–256 + 368.(in Chinese)
48. Xue G, Li X, Di Q (2007) The progress of TEM in theory and application.Progress in Geophysics1195–1200
49. Yan S, Shi X, Chen M (2009) The probing depth of transient electromagnetic field method. Chin J Geophys 52:1583–1591. https://doi.org/10.3969/j.issn.0001-5733.2009.06.020
50. Yao W, Li W, Zhang W (2012) Multi-electrode resistivity method and ground penetrating radar (GPR) in the karst exploration in Kunming Changshui international airport. Sci Technol Eng 12:8175–8179
51. Yin X, Kong G, Zhang G (2008) Seismic attributes optimization based on kernel principal component analysis (KPCA) and application. Oil Geophysical Prospecting 179–183 + 124–125 + 246

52. Zhang J, Liu S, Chen Q, Wang B, Ren C (2019) Application of cross-borehole integrated geophysical methods for the detailed investigation of karst in urban metro construction. J Environ Eng Geoph 24:525–536. https://doi.org/10.2113/jeeg24.04.03.525
53. Zhou Y, Zhang G, Gao G, Zhao W, Yi Y, Wei H (2019) Application of kernel principal component analysis in well logging turbidite lithology identification. Oil Geophys Prospect 54:667–675

Figures

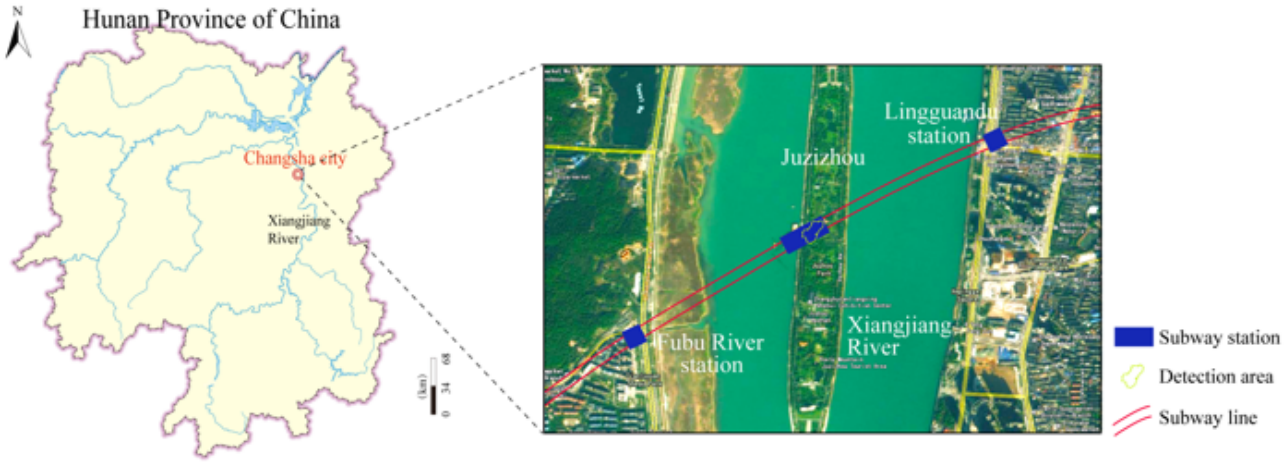

Figure 1

Location of the study area

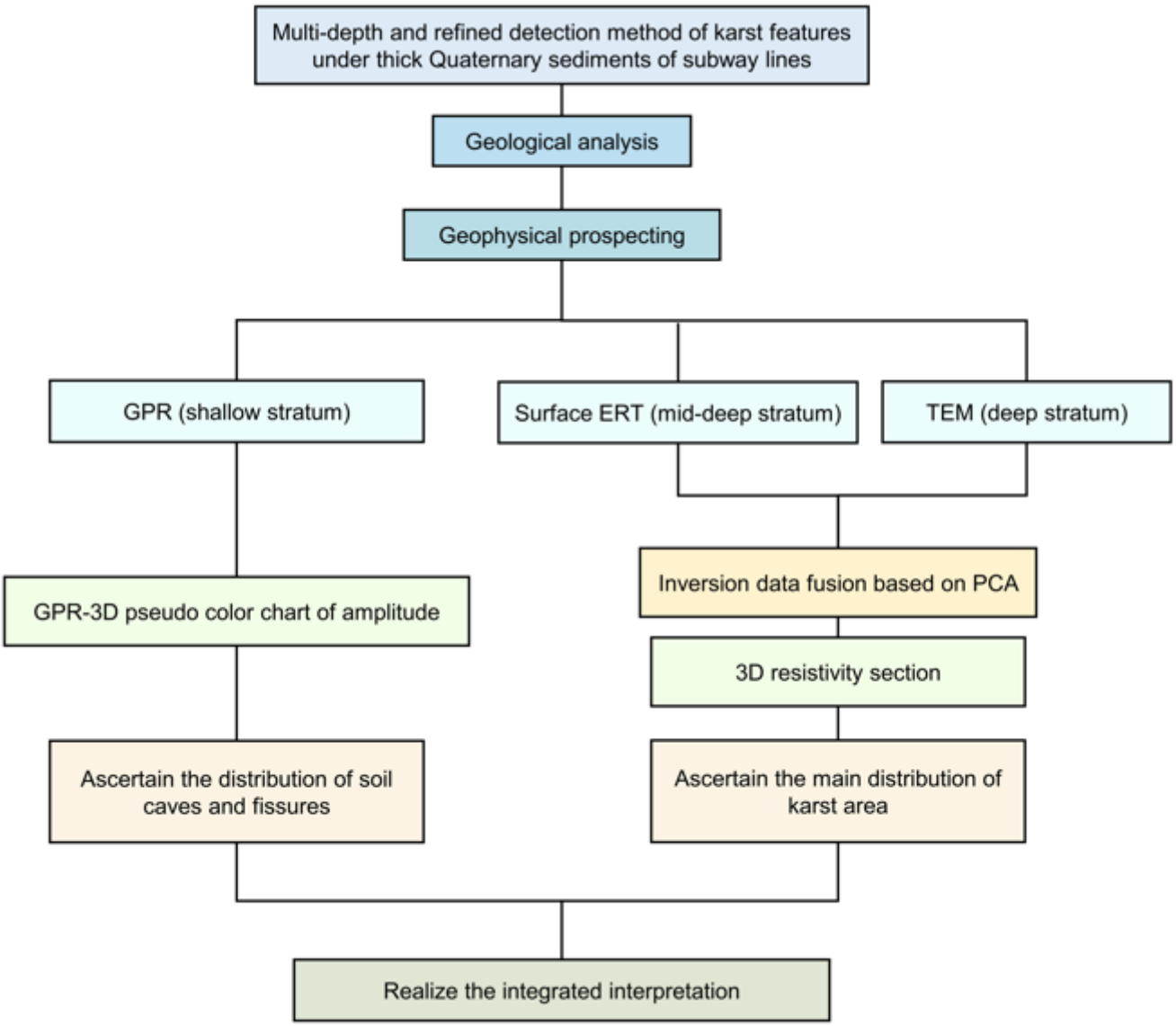

Figure 2

Schematic of the technology roadmap multi-depth and refined detection method of karst features under thick Quaternary sediments of subway lines

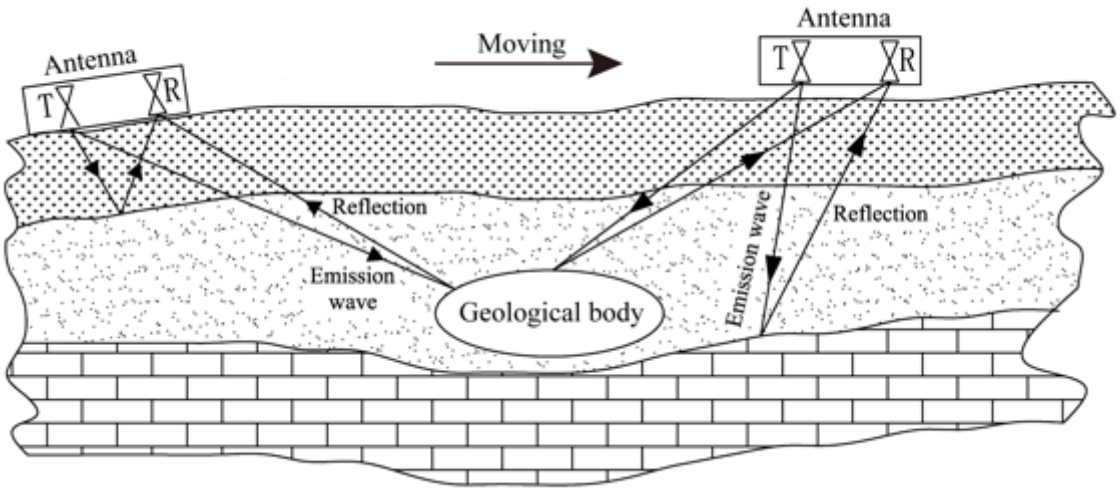

Figure 3

Schematic diagram of GPR method

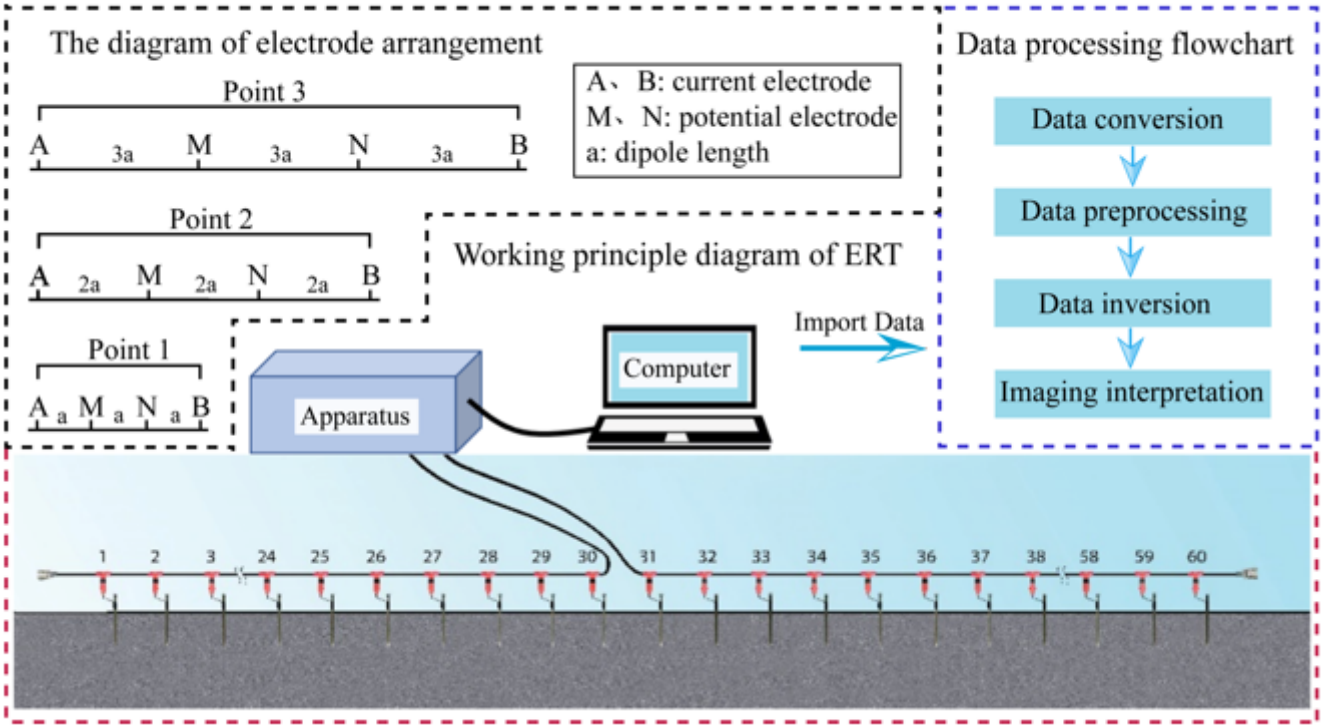

Figure 4

Schematic diagram of the surface ERT method, electrode arrangement and data processing flowchart

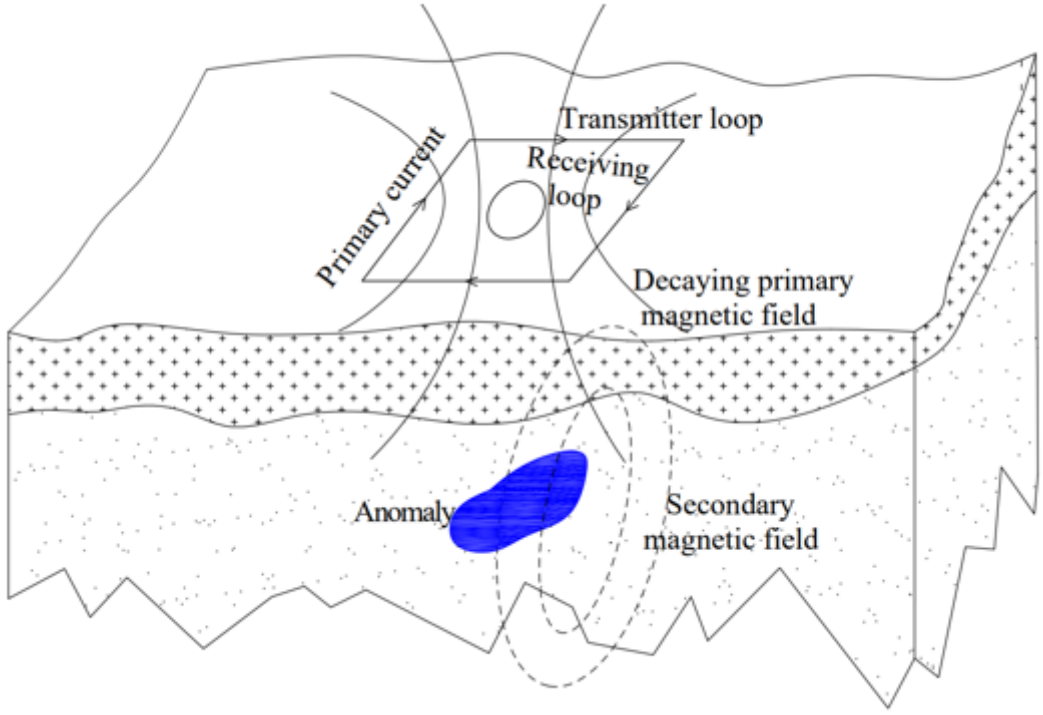

Figure 5

Schematic diagram of the TEM method

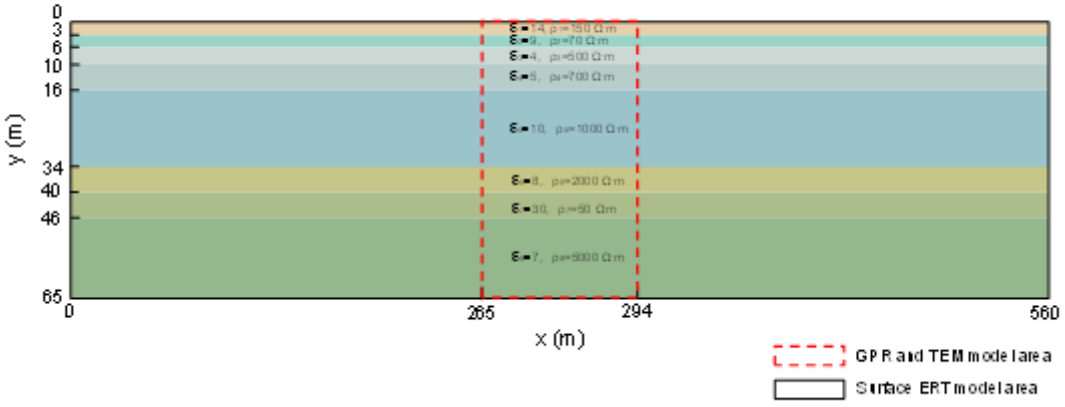

Figure 6

Model of numerical simulation

Figure 7

Numerical simulation of eight stratums using GPR

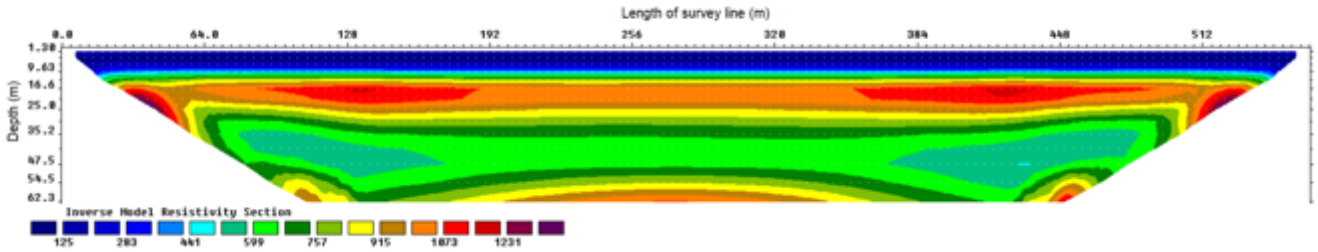

Figure 8

Numerical simulation of eight stratums using surface ERT

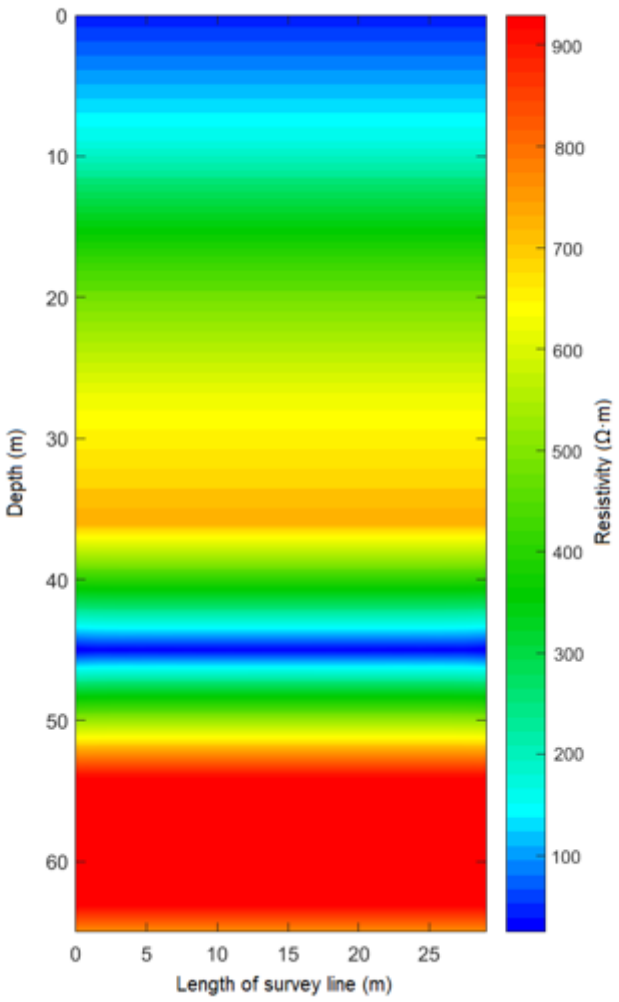

Figure 9

Numerical simulation of eight stratums using TEM

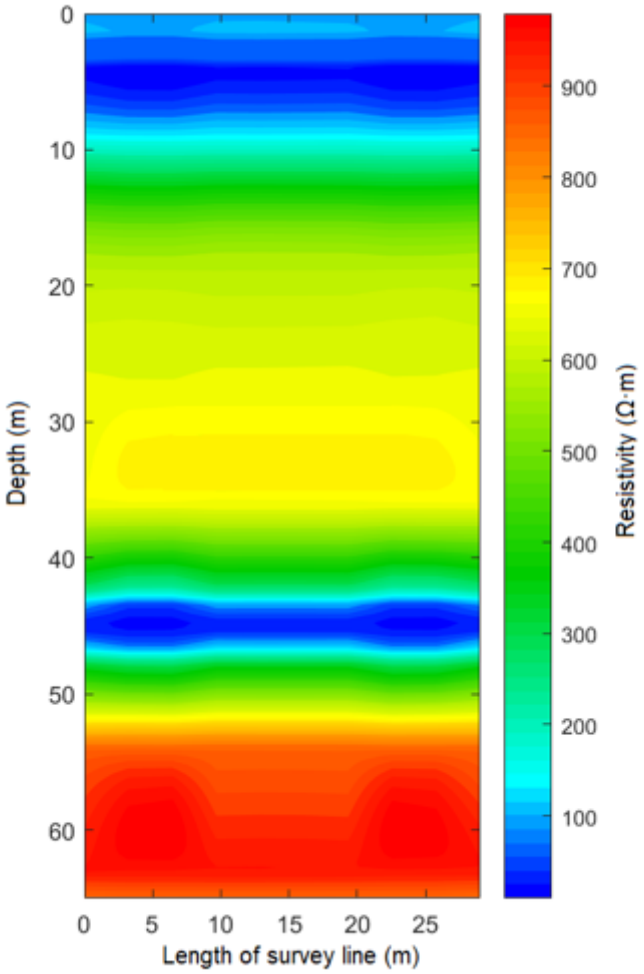

Figure 10

Cross-section after TEM and surface ERT inversion resistivity data fusion

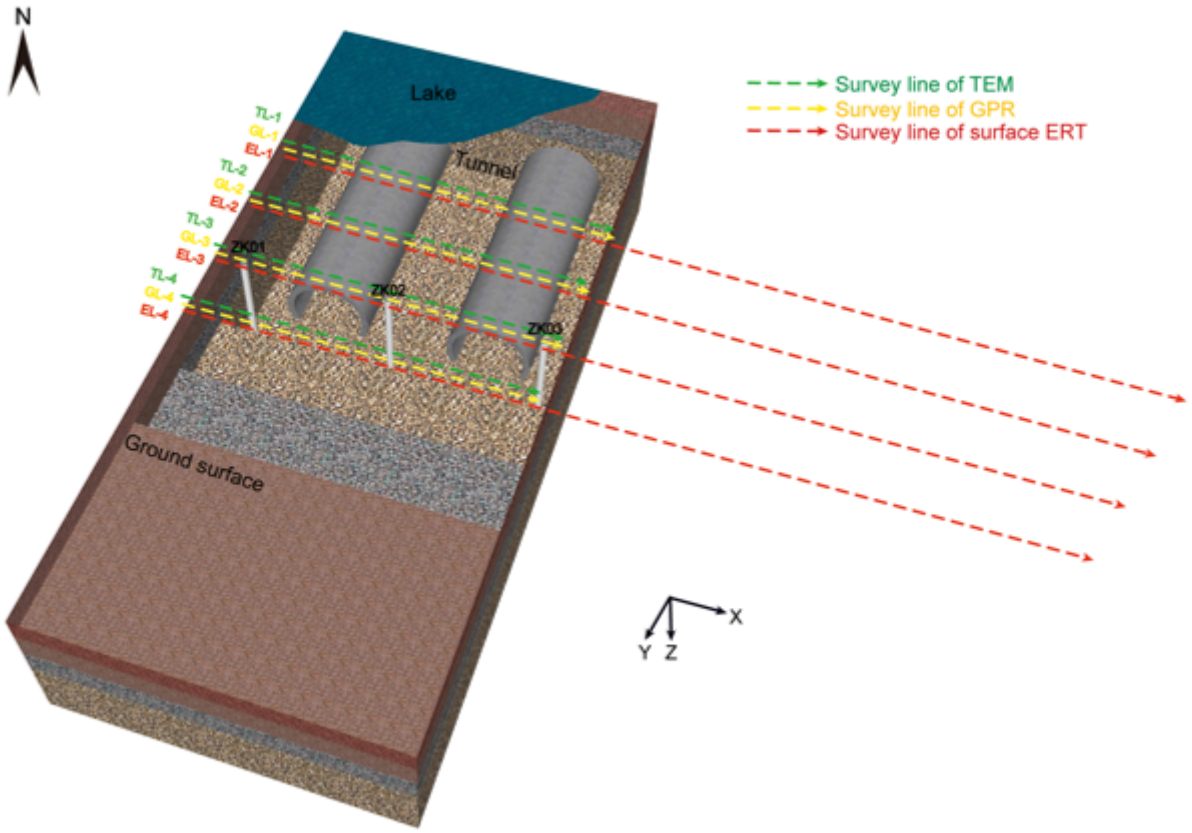

Figure 11

Layout of the survey line

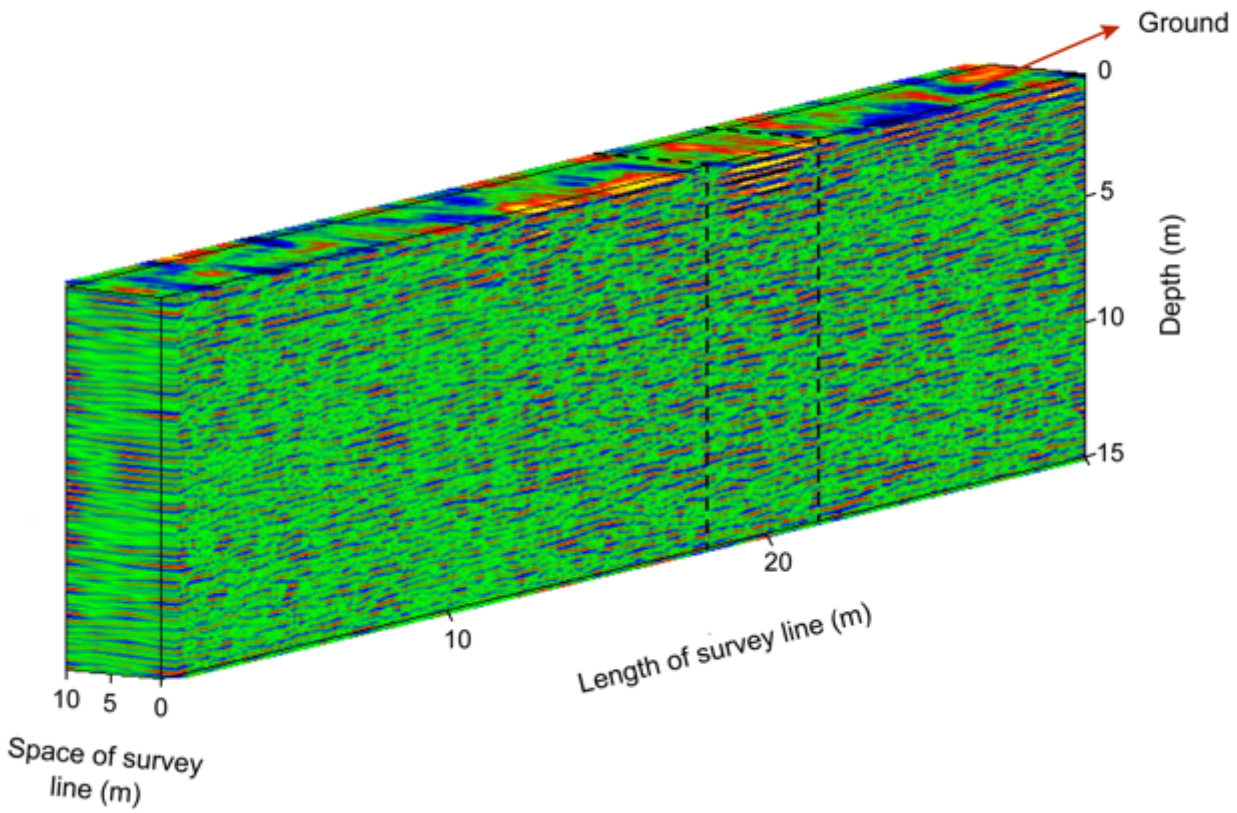

Figure 12

3D pseudo-colour waveform results of GPR

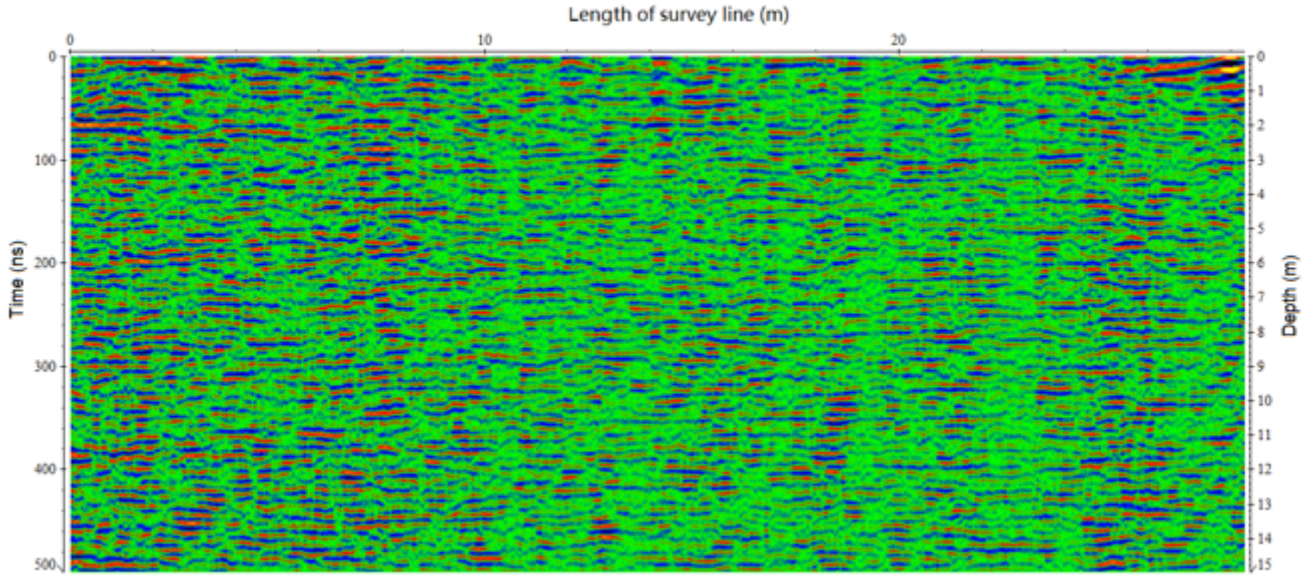

Figure 13

2D GPR slice for detailed interpretation of geological structures at GL-4

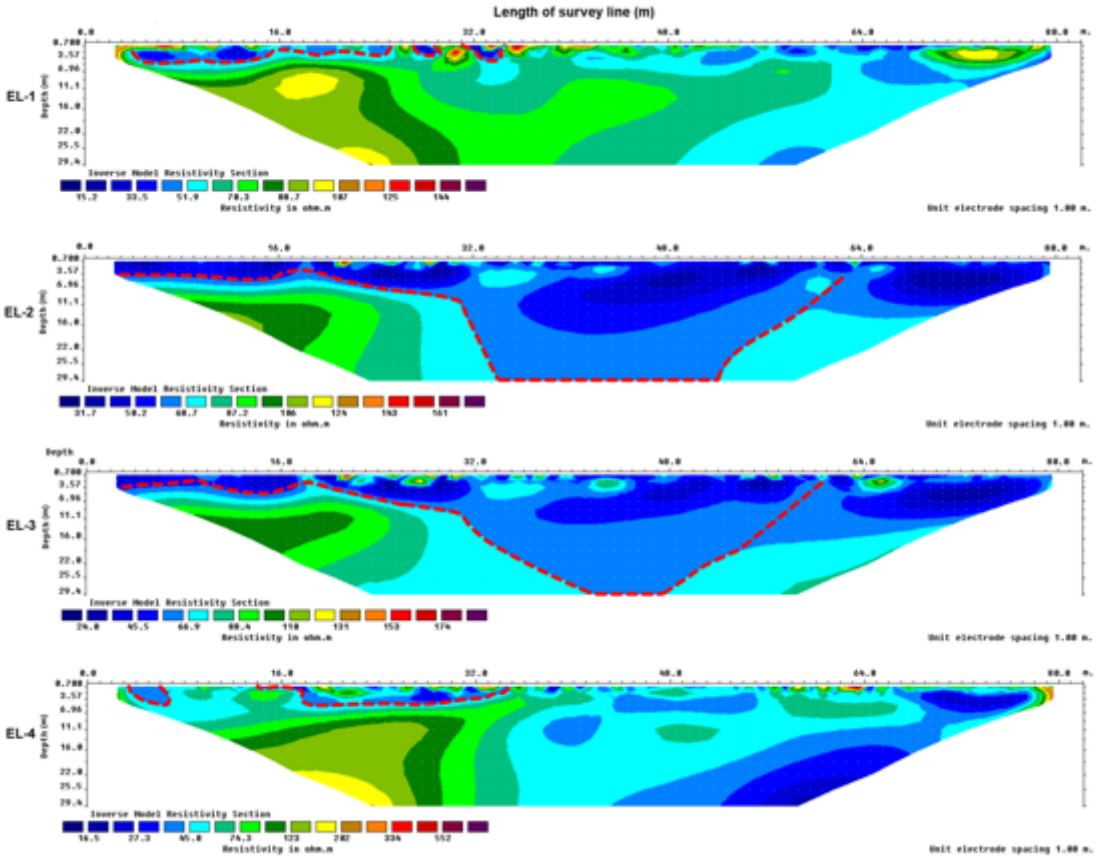

Figure 14

Surface ERT inversion section

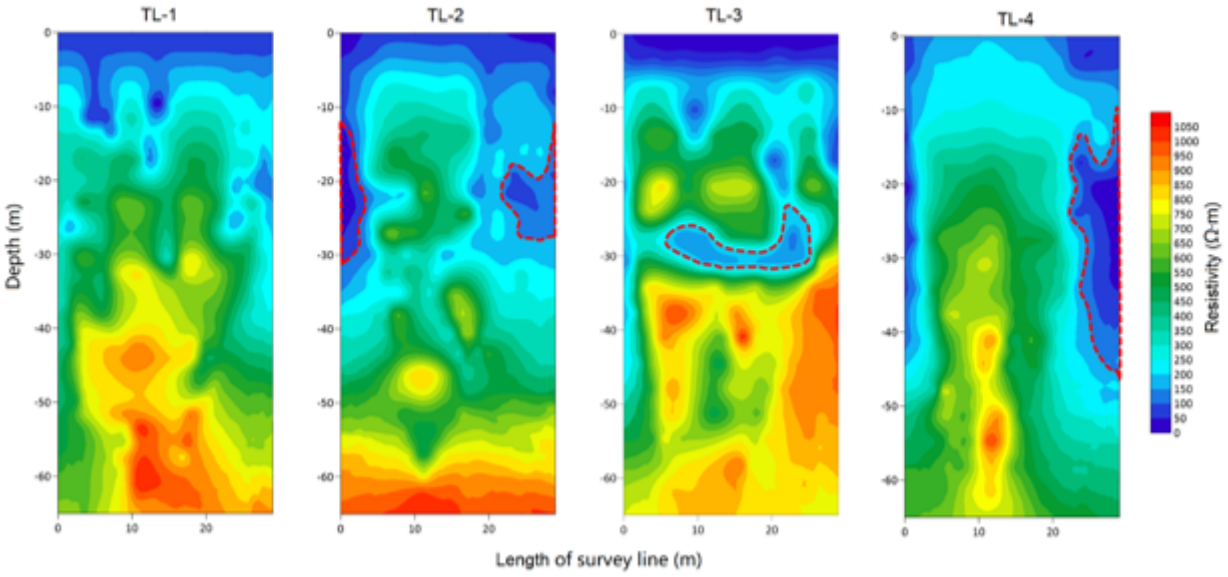

Figure 15

TEM inversion results

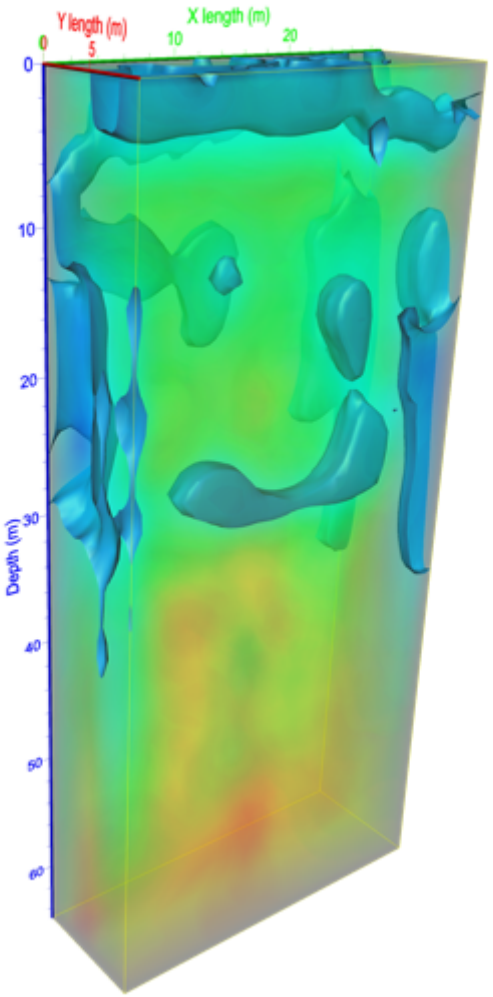

Figure 16

Resistivity fusion 3D imaging

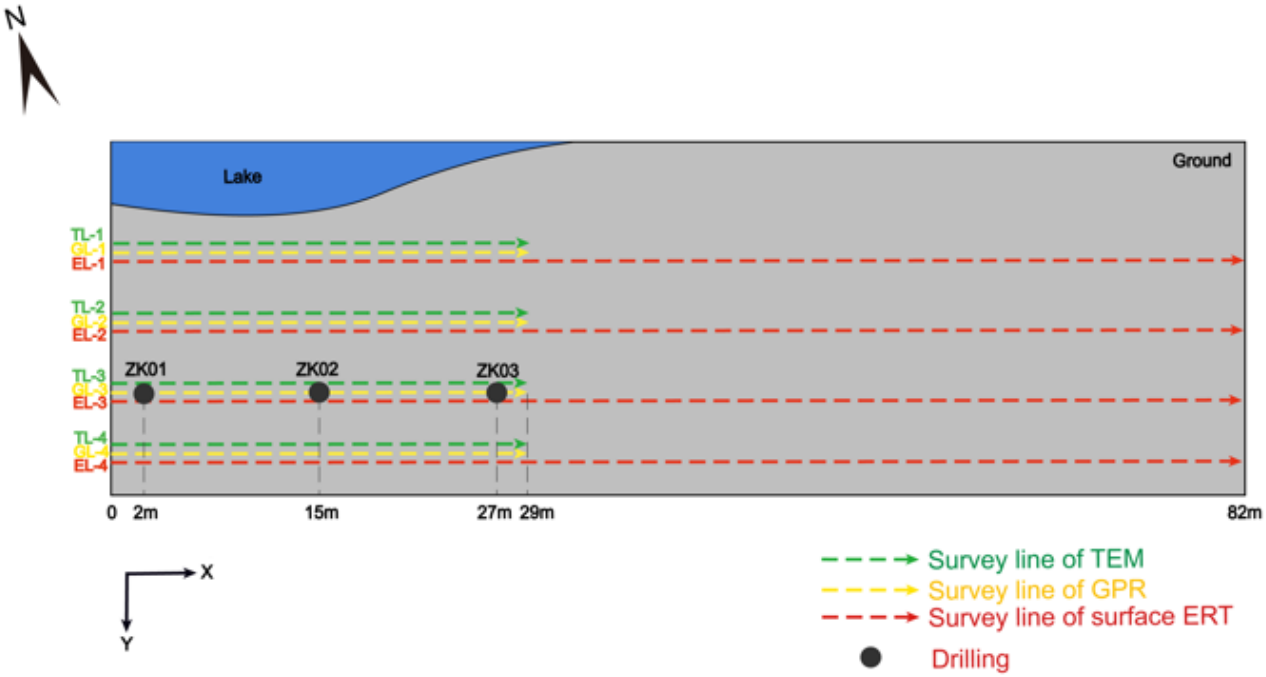

Figure 17

Drilling position map of the study area

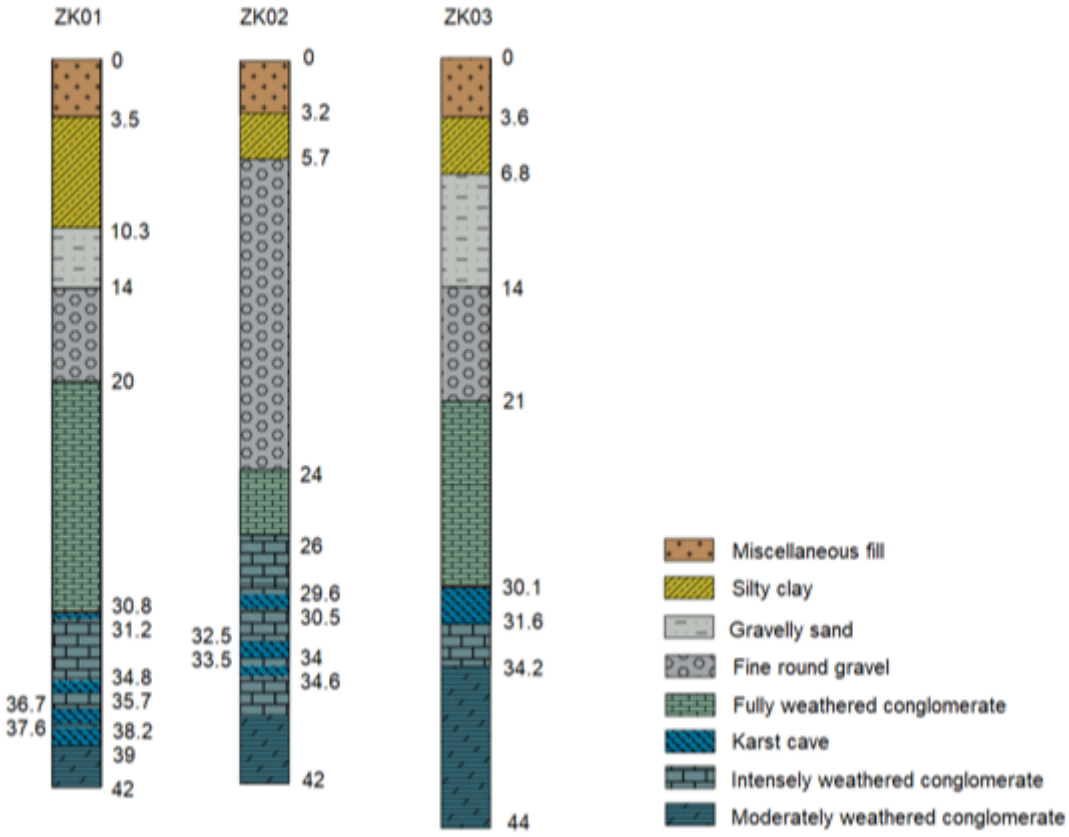

Figure 18

Drilling histograms of the engineering site: each drilling corresponds to the specific position in Fig. 17